Overlap QRM-ML Block Signal Detection for Single-Carrier Transmission without CP Insertion

Hideyuki MOROGA† Tetsuya YAMAMOTO† and Fumiyuki ADACHI‡
Dept. of Electrical and Communication Engineering, Graduate School of Engineering, Tohoku University
6-6-05 Aza-Aoba, Aramaki, Aoba-ku, Sendai, 980-8579 Japan
†{moroga, yamamoto}@mobile.ecei.tohoku.ac.jp, ‡adachi@ecei.tohoku.ac.jp

***Abstract*— A block signal maximum likelihood detection (MLD) employing QR decomposition and M-algorithm (QRM-MLBD) can significantly improve the bit error rate (BER) performance of the single carrier (SC) transmissions in a frequency-selective fading channel, compared to the conventional frequency-domain equalization (FDE). In QRM-MLBD, the cyclic prefix (CP) is inserted in order to avoid inter-block interference (IBI). However, the CP insertion reduces the transmission efficiency. In this paper, we propose an overlap QRM-MLBD which requires no CP insertion. In overlap QRM-MLBD, IBI can be suppressed by overlapping consecutive observation windows and picking up only the reliable part after the block signal detection. We evaluate the average BER performance and the throughput performance by computer simulation to compare with the conventional QRM-MLBD with CP insertion.**

Keywords; Single-carrier, QRM-MLBD, time-domain signal detection, no gurard interval

I. INTRODUCTION

In next generation mobile communication systems, high data rate wireless communication systems are demanded for advanced services. However, since the wireless channel is composed of many propagation paths with different time delays, the channel becomes severely frequency-selective. In a severe frequency-selective fading channel, the bit error rate (BER) performance significantly degrades due to inter-symbol interference (ISI) when single-carrier (SC) transmission without equalization is used [1, 2].

The conventional minimum mean square error based frequency-domain equalization (MMSE-FDE) improves the SC transmission performance [3, 4], but it exhibits still a big performance gap from MF bound [5].

A frequency-domain block signal maximum likelihood detection (MLD) employing QR decomposition and M-algorithm (FD-QRM-MLBD) [6, 7] can significantly improve the BER performance of SC block transmissions compared to the MMSE-FDE. In FD-QRM-MLBD, the discrete Fourier transform (DFT) of the received signal is required. FD-QRM-MLBD is equivalent to time-domain implementation of QRM-MLBD (TD-QRM-MLBD) [8]. Since TD-QRM-MLBD does not require DFT of the received signal, its computational complexity is lower than that of FD-QRM-MLBD.

In the conventional SC block transmission, the insertion of cyclic prefix (CP) is used to avoid the inter-block interference (IBI) and make the received signal block to be a circular convolution of the transmitted block and channel impulse response. However, CP insertion reduces transmission efficiency. Therefore, an overlap MMSE-FDE which requires no CP insertion was proposed [9, 10]. However, it exhibits still a big performance gap from MF bound.

Without CP insertion, the performance of QRM-MLBD degrades due to the IBI. The IBIs are stronger on symbols near the both ends of block. In this paper, we propose an overlap QRM-MLBD which suppresses the IBI. QRM-MLBD is applied to the received signal over the observation window. Then, only the reliable symbols are picked up to suppress the IBI. To detect a continuously transmitted symbol stream, the present observation window overlaps with previous and next observation windows. In this paper, we will investigate the average BER performance and the throughput performance achievable by overlap QRM-MLBD by computer simulation to compare with the conventional QRM-MLBD with CP insertion. We will also discuss the computational complexity of the proposed overlap QRM-MLBD. Therefore, the transmission efficiency is higher than that of the conventional QRM-MLBD.

The remainder of this paper is organized as follows. Sect. II presents the proposed overlap QRM-MLBD. In Sect. III, the BER performance and the throughput performance are evaluated by computer simulation. Computational complexity of the overlap QRM-MLBD is also discussed. Section IV concludes this paper.

II. OVERLAP QRM-MLBD

A. Transmission system

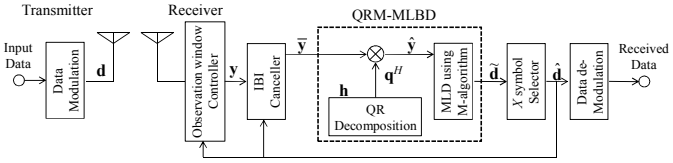

Figure 1. SC transmission using overlap QRM-MLBD.

Figure 1 shows the system model of SC transmission using overlap QRM-MLBD. Figure 2 shows block signal processing of overlap QRM-MLBD. Throughout the paper, the equivalent low-pass representation of discrete-time t normalized by the transmission symbol length T_s is used.

At the receiver, the received signal is divided into a sequence of blocks of X symbols to be picked up (called X-symbol block). Then, the received signal $\mathbf{y}=[y(0),...,y(t),...,y(N_c+L-2)]^T$ of N_c+L-1 symbols (called the observation window) is stored to detect a block of N_c symbols including X-symbol block at the beginning, where L is the number of propagation paths. The IBI from the previous block is removed by generating its replica and subtracting it from the

978-1-4673-0990-5/12/$31.00 ©2012 IEEE

received signal sequence over the observation window before applying QRM-MLBD. After QRM-MLBD, the first X-symbol block is picked up. To detect the next X-symbol block, the observation window is shifted by X-symbol block as shown in Fig. 2. By repeating this process, the continuously transmitted symbol sequence can be detected.

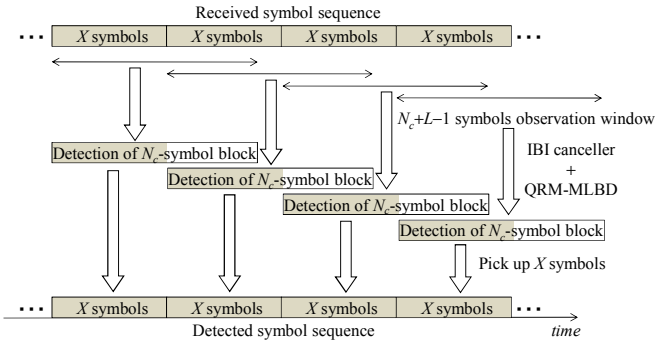

Figure 2. Overlap QRM-MLBD.

B. Received signal representation

The SC signal is transmitted over a frequency-selective fading channel composed of L propagation paths with different time delays. The channel impulse response $h(\tau)$ can be expressed as

$$h(\tau)=\sum_{l=0}^{L-1} h_l \delta(\tau-\tau_l), \tag{1}$$

where h_l and τ_l are respectively the complex-valued path gain with $E[\sum_{l=0}^{L-1}|h_l|^2]=1$ and the time delay of the lth path. The lth path time delay is assumed to be l symbols (i.e., $\tau_l=l$) and the path gains remain constant over at least an interval of the observation window. The received signal sequence $\mathbf{y}=[y(0),...,y(t),...,y(N_c+L-2)]^T$ of N_c+L-1 symbols in the observation window can be expressed using the matrix form as

$$\mathbf{y}=\sqrt{\frac{2E_s}{T_s}}\mathbf{h}\mathbf{d}+\sqrt{\frac{2E_s}{T_s}}\mathbf{h}_{-1}\mathbf{d}_{-1}+\sqrt{\frac{2E_s}{T_s}}\mathbf{h}_{+1}\mathbf{d}_{+1}+\mathbf{n}, \tag{2}$$

where $\mathbf{h}$, $\mathbf{h}_{-1}$, and $\mathbf{h}_{+1}$ are respectively an $(N_c+L-1)\times N_c$ channel impulse response matrixes given as

$$\begin{cases} \mathbf{h}=\begin{bmatrix} h_0 & & \mathbf{0} \\ \vdots & \ddots & \\ h_{L-1} & & \ddots \\ & \ddots & h_0 \\ & & \vdots \\ \mathbf{0} & & h_{L-1} \end{bmatrix}, \\ \mathbf{h}_{-1}=\begin{bmatrix} & h_{L-1} & \cdots & h_1 \\ & & \ddots & \vdots \\ & & & h_{L-1} \\ & \mathbf{0} & & \end{bmatrix}, \mathbf{h}_{+1}=\begin{bmatrix} & & & \mathbf{0} \\ & & & \\ h_0 & & & \\ \vdots & \ddots & & \\ h_{L-2} & \cdots & h_0 & \end{bmatrix}. \end{cases} \tag{3}$$

$\mathbf{d}=[d(0),...,d(t),...,d(N_c-1)]^T$ represents the desired transmit symbol sequence. $\mathbf{d}_{-1}=[d_{-1}(0),...,d_{-1}(t),...,d_{-1}(N_c-1)]^T$ and $\mathbf{d}_{+1}=[d_{+1}(0),...,d_{+1}(t),...,d_{+1}(N_c-1)]^T$ represent the transmit symbol sequences in the previous block and in the next block, respectively. The first term of Eq. (2) represents the desired signal component. The second and the third terms represent the IBI components from the previous block and from the next block, respectively. $\mathbf{n}=[n(0),...,n(t),...,n(N_c+L-2)]^T$ is the noise vector. The tth element, $n(t)$, of $\mathbf{n}$ is the zero-mean complex Gaussian variable having the variance $2N_0/T_s$ with N_0 being the one-sided power spectrum density of the additive white Gaussian noise (AWGN). E_s is the transmit symbol energy.

C. Overlap QRM-MLBD

The IBI replica from the previous block is generated by using the decision of $\hat{\mathbf{d}}_{-1}=[\hat{d}_{-1}(0),...,\hat{d}_{-1}(t),...,\hat{d}_{-1}(N_c-1)]^T$ of the previous block. The IBI cancellation is performed by subtracting the IBI replica from the received signal as

$$\begin{aligned} \overline{\mathbf{y}} &= \mathbf{y}-\sqrt{\frac{2E_s}{T_s}}\mathbf{h}_{-1}\hat{\mathbf{d}}_{-1} \\ &= \sqrt{\frac{2E_s}{T_s}}\mathbf{h}\mathbf{d}+\sqrt{\frac{2E_s}{T_s}}\mathbf{h}_{-1}\left(\mathbf{d}_{-1}-\hat{\mathbf{d}}_{-1}\right)+\sqrt{\frac{2E_s}{T_s}}\mathbf{h}_{+1}\mathbf{d}_{+1}+\mathbf{n}, \end{aligned} \tag{4}$$

where the second term of Eq.(4) is the residual IBI from the previous block.

In overlap QRM-MLBD, QR decomposition is applied to the channel impulse response matrix of the desired signal component $\mathbf{h}$ as

$$\mathbf{h}=\mathbf{q}\mathbf{r}, \tag{5}$$

where $\mathbf{q}$ is an $(N_c+L-1)\times N_c$ unitary matrix satisfying $\mathbf{q}^H\mathbf{q}=\mathbf{I}$ ($\mathbf{I}$ is the identity matrix) and $\mathbf{r}$ is an $N_c\times N_c$ upper triangular matrix. $(.)^H$ denotes the Hermitian transpose operation. By left multiplying $\mathbf{q}^H$ to $\overline{\mathbf{y}}$, we obtain the transformed vector given by

$$\begin{aligned} \hat{\mathbf{y}} &= \mathbf{q}^H\overline{\mathbf{y}} \\ &= \sqrt{\frac{2E_s}{T_s}}\mathbf{r}\mathbf{d}+\sqrt{\frac{2E_s}{T_s}}\hat{\mathbf{h}}_{-1}\left(\mathbf{d}_{-1}-\hat{\mathbf{d}}_{-1}\right)+\sqrt{\frac{2E_s}{T_s}}\hat{\mathbf{h}}_{+1}\mathbf{d}_{+1}+\hat{\mathbf{n}}, \end{aligned} \tag{6}$$

where $\hat{\mathbf{h}}_{-1}=\mathbf{q}^H\mathbf{h}_{-1}$, $\hat{\mathbf{h}}_{+1}=\mathbf{q}^H\mathbf{h}_{+1}$, and $\hat{\mathbf{n}}=\mathbf{q}^H\mathbf{n}$. From Eq. (6), ML solution can be expressed as

$$\tilde{\mathbf{d}}_{ML}=\arg\min_{\mathbf{d}\in Z^{N_c}}\left\|\hat{\mathbf{y}}-\sqrt{\frac{2E_s}{T_s}}\mathbf{r}\overline{\mathbf{d}}\right\|^2, \tag{7}$$

where Z is the modulation level (e.g., Z=4 for quaternary phase shift keying (QPSK) and Z=16 for 16-quadrature amplitude modulation (QAM)). $\overline{\mathbf{d}}$ is the candidate symbol vector. Thanks to the upper triangular structure of $\mathbf{r}$, M MLD can be done using a N_c-stages M-algorithm [11] to reduce the computational complexity. The M-algorithm keeps only M most reliable paths as surviving paths at each stage. The most likely transmitted symbol sequence is found by tracing back the surviving path having the smallest accumulated path metric at the last stage.

Without CP insertion, the IBI from both the previous and the next blocks is present. The IBI from the previous block can

be suppressed by using the decision of the previous block as Eq.(4). However, the IBI from the next block cannot be removed. Here, we consider the distribution of IBI from the next block after multiplying $\mathbf{q}^H$. The channel impulse response matrix of the desired signal $\mathbf{h}$ is is shown in Eq. (3). Therefore, the unitary matrix $\mathbf{q}$ and the upper triangular matrix $\mathbf{r}$ obtained by QR decomposition of $\mathbf{h}$ are represented as

$$\begin{cases} \mathbf{q} = \begin{bmatrix} q_{0,0} & \cdots & \cdots & \cdots & q_{N_c-1,0} \\ \vdots & & & & \vdots \\ q_{0,L-1} & & & & \vdots \\ & \ddots & & & \vdots \\ & & \ddots & & \vdots \\ & & & \ddots & \vdots \\ \mathbf{0} & & & & q_{N_c-1,N_c+L-2} \end{bmatrix}. \\ \mathbf{r} = \begin{bmatrix} r_{0,0} & \cdots & r_{L-1,0} & & \mathbf{0} \\ & \ddots & & \ddots & \\ & & \ddots & & r_{N_c-L,N_c-1} \\ & & & \ddots & \vdots \\ \mathbf{0} & & & & r_{N_c-1,N_c-1} \end{bmatrix} \end{cases} \quad (8)$$

From Eq. (8), the IBI from the next block (third term of Eq. (6)) can be given as

$$\sqrt{\frac{2E_s}{T_s}}\hat{\mathbf{h}}_{+1}\mathbf{d}_{+1} = \sqrt{\frac{2E_s}{T_s}}\mathbf{q}^H\mathbf{h}_{+1}\mathbf{d}_{+1}$$
$$= \sqrt{\frac{2E_s}{T_s}}\begin{bmatrix} & & & \mathbf{0} \\ & & & \\ \hat{h}_{+1\,N_c-L+1,0} & & & \\ \vdots & & \ddots & \\ \hat{h}_{+1\,N_c-1,0} & & \cdots & \hat{h}_{+1\,N_c-1,L-1} \end{bmatrix}\begin{bmatrix} d_{+1}(0) \\ \vdots \\ \vdots \\ d_{+1}(N_c-1) \end{bmatrix}. \quad (9)$$

It can be seen from Eq. (9) that the IBI from the next block exists only near the end of the transformed signal. Figure 3 plots the average IBI power from the next block, normalized by the transmit power. The number of symbols to be detected is assumed to be N_c=64. The IBI power containing the tth transformed received signal $\hat{y}(t)$ can be given by $E[\sum_{j=0}^{N_c-1}|\hat{h}_{+1\,i,j}|^2]$.

It can be understood from Fig. 3 that the IBI exists only on the last $L-1$ symbols of the transformed signal. The IBI is more significant at early stages in the M-algorithm. Therefore, the probability of removing the correct path is high at early stages of the M-algorithm due to the stronger IBI. On the other hand, the IBI is less significant at later stages of the M-algorithm. Furthermore, the upper-right elements of the upper triangular matrix of Eq. (8) are 0. Therefore, the effect of the removing the correct path at early stages does not affect the path selection at last stages. As a result, decision on the symbols corresponding to the last stages is more reliable.

Figure 4 shows the average symbol error rate (SER) for 16QAM data modulation, N_c=64, M=16. L=16 path uniform power delay profile is assumed. Perfect IBI cancellation from the previous block is assumed. It can be seen from Fig. 4 that SER is higher for the symbols towards the end of block. SER is lower for the symbols towards the beginning of the block. Therefore, only the reliable first X-symbol block $\hat{\mathbf{d}} = [\tilde{d}(0),..,\tilde{d}(t),..,\tilde{d}(X-1)]^T$ is picked up from the detected symbol sequence $\tilde{\mathbf{d}} = [\tilde{d}(0),...,\tilde{d}(t),...,\tilde{d}(N_c-1)]^T$.

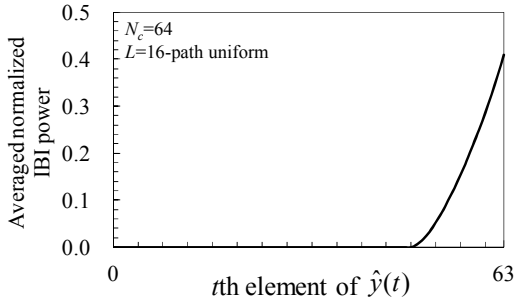

Figure 3. Averaged normalized IBI power associated with the tth element of $\hat{y}(t)$.

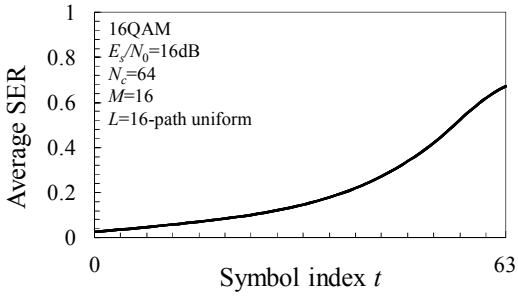

Figure 4. Average SER.

D. Equivalence between overlap time-domain QRM-MLBD and overlap frequency-domain QRM-MLBD

In this subsection, we show the equivalence between the overlap time-domain QRM-MLBD (overlap TD-QRM-MLBD) and overlap frequency-domain QRM-MLBD (overlap FD-QRM-MLBD). Applying an N_c+L-1-point DFT to Eq. (4), the frequency domain received signal $\overline{\mathbf{Y}} = [\overline{Y}(0),...,\overline{Y}(t),...,\overline{Y}(N_c-1)]^T$ after IBI cancellation can be expressed using the matrix form as

$$\overline{\mathbf{Y}} = \sqrt{\frac{2E_s}{T_s}}\mathbf{H}\mathbf{d} + \sqrt{\frac{2E_s}{T_s}}\mathbf{H}_{-1}\left(\mathbf{d}_{-1} - \hat{\mathbf{d}}_{-1}\right) + \sqrt{\frac{2E_s}{T_s}}\mathbf{H}_{+1}\mathbf{d}_{+1} + \mathbf{N}, \quad (10)$$

where $\mathbf{H}_{-1}$, $\mathbf{H}$, and $\mathbf{H}_{+1}$ are the frequency domain equivalent channel matrixes and can be expressed using a $(N_c+L-1)\times(N_c+L-1)$ DFT matrix $\mathbf{F}$ as $\mathbf{H}=\mathbf{F}\mathbf{h}$, $\mathbf{H}_{-1}=\mathbf{F}\mathbf{h}_{-1}$ and $\mathbf{H}_{+1}=\mathbf{F}\mathbf{h}_{+1}$, respectively.

QR decomposition is applied to the desired signal component $\mathbf{H}$ as

$$\mathbf{H} = \mathbf{Q}\mathbf{R}, \quad (11)$$

where $\mathbf{Q}$ is a $(N_c+L-1)\times N_c$ unitary matrix satisfying $\mathbf{Q}^H\mathbf{Q}=\mathbf{I}$ ($\mathbf{I}$ is the identity matrix) and $\mathbf{R}$ is an $N_c\times N_c$ upper triangular matrix. By left multiplying $\mathbf{Q}^H$ to $\overline{\mathbf{Y}}$, we have the transformed vector given by

$$\hat{\mathbf{Y}} = \mathbf{Q}^H \overline{\mathbf{Y}} = \sqrt{\frac{2E_s}{T_s}}\mathbf{R}\mathbf{d} + \sqrt{\frac{2E_s}{T_s}}\hat{\mathbf{H}}_{-1}\left(\mathbf{d}_{-1} - \hat{\mathbf{d}}_{-1}\right) + \sqrt{\frac{2E_s}{T_s}}\hat{\mathbf{H}}_{+1}\mathbf{d}_{+1} + \hat{\mathbf{N}}, \tag{12}$$

where $\hat{\mathbf{H}}_{-1} = \mathbf{Q}^H \mathbf{H}_{-1}$, $\hat{\mathbf{H}}_{+1} = \mathbf{Q}^H \mathbf{H}_{+1}$ and $\hat{\mathbf{N}} = \mathbf{Q}^H \mathbf{N}$.

By left multiplying **F** to Eq. (5), we have **Fh=Fqr**. Since **F** and **q** are unitary matrixes, **Fq** is also unitary matrix. Since QR decomposition is unique and **Fh=H**, we obtain the following equations from Eqs. (5) and (11), given by

$$\begin{cases} \mathbf{Fq} = \mathbf{Q} \\ \mathbf{r} = \mathbf{R} \end{cases}. \tag{13}$$

The received signal $\hat{\mathbf{y}}$ is transformed by using Eqs. (12) and (13) as

$$\hat{\mathbf{y}} = \mathbf{q}^H \overline{\mathbf{y}} = \mathbf{q}^H \mathbf{F}^H \mathbf{F}\overline{\mathbf{y}} = \left(\mathbf{Fq}\right)^H \left(\mathbf{F}\overline{\mathbf{y}}\right) = \mathbf{Q}^H \overline{\mathbf{Y}} = \hat{\mathbf{Y}} \tag{14}$$

Similarly,

$$\begin{cases} \hat{\mathbf{h}}_{-1} = \mathbf{Q}^H \mathbf{H}_{-1} = \hat{\mathbf{H}}_{-1} \\ \hat{\mathbf{h}}_{+1} = \mathbf{Q}^H \mathbf{H}_{-1} = \hat{\mathbf{H}}_{+1} \\ \hat{\mathbf{n}} = \mathbf{Q}^H \mathbf{N} = \hat{\mathbf{N}} \end{cases}. \tag{15}$$

From Eqs. (6) and (12)-(15), it can be understood that overlap TD-QRM-MLBD is equivalent to overlap FD-QRM-MLBD.

The overlap FD-QRM-MLBD requires the DFT and the calculation of the equivalent channel matrix **H**. Therefore, the computational complexity of the overlap FD-QRM-MLBD is bigger than that of the overlap TD-QRM-MLBD. Therefore, in this paper, only overlap TD-QRM-MLBD is considered.

III. Computer Simulation

We consider 16QAM data modulation, packet size N_p=192, and GI length N_g=0. X symbols are assumed to be picked up from the N_c=64 symbols to be detected, The channel is assumed to be a frequency-selective block Rayleigh fading channel having L=16-path uniform power delay profile and the normalized time delay $\tau_l = l$. We assume that there is no fading variation in one packet and ideal channel estimation is assumed.

A. BER performance and throughput performance

Figure 5 plots the average BER performance of SC transmission using overlap QRM-MLBD as a function the average received bit energy-to-noise power spectrum density ratio $E_b/N_0 = 0.25(E_s/N_0)(1+N_g/N_c)$. We consider the number of surviving paths M=16. The average BER performance of the conventional QRM-MLBD with CP insertion is also plotted for comparison. We use the training sequence (TS) aided QRM-MLBD with GI length of 16 symbols [12] as the conventional QRM-MLBD with CP insertion.

It can be seen from Fig. 5 that in overlap QRM-MLBD, the BER performance improves by reducing X. This is because at last stages of M-algorithm, the IBI from the next block is less significant. Furthermore, removing the correct path at early stages does not affect the path selection. Furthermore, the IBI cancellation is improved. When X=4, overlap QRM-MLBD achieves better BER performance than the conventional QRM-MLBD with CP insertion. This is because overlap QRM-MLBD has no GI insertion loss while the conventional QRM-MLBD has the power loss caused by CP insertion.

Figure 6 plots the throughput performance as a function of average received E_s/N_0. Throughput is defined as $\log_2 Z \times (1-\text{PER})/(1+N_g/N_c)$, where PER denotes the packet error rate. It can be seen from Fig. 6 that in overlap QRM-MLBD, the throughput performance improves by reducing X. When M=16, overlap QRM-MLBD with $X \le 16$ achieve higher throughput than the conventional QRM-MLBD with CP insertion. Since overlap QRM-MLBD does not require the CP insertion, the throughput is higher than that of the conventional QRM-MLBD with CP insertion. Consequently, the peak throughput is obtained, which is 1.25 times higher than that of the conventional QRM-MLBD with CP insertion.

The required number X of symbols to be picked up to achieve sufficiently improved throughput performance is discussed below. The throughput performance is plotted as a function of X when E_s/N_0=22dB as shown in Fig. 7. The required E_s/N_0 to achieve the peak throughput is 22dB for the conventional QRM-MLBD with CP insertion. The required X for achieving higher throughput than the conventional QRM-MLBD with CP insertion is X=16 when $M \ge 4$ and is X=8 when $M \ge 16$.

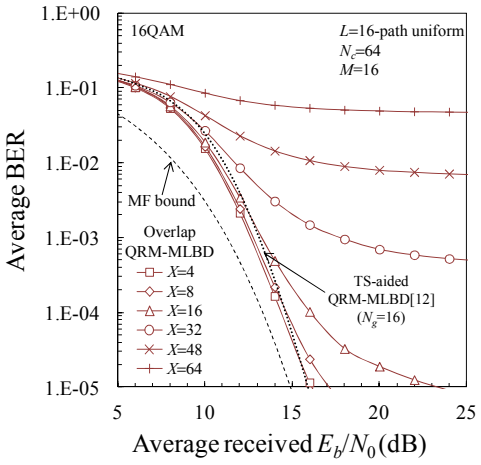

Figure 5. BER performance.

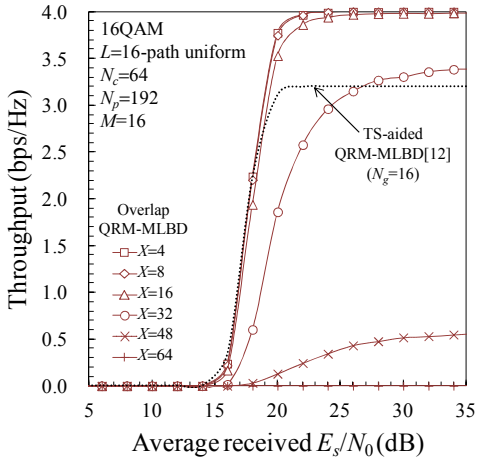

Figure 6. Throughput performance.

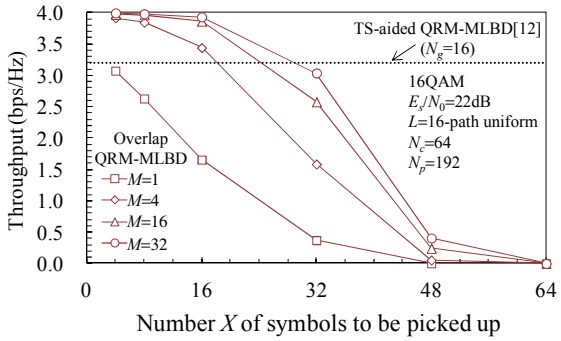

Figure 7. Impact of X on throughput.

B. Computational complexity

Table1. Number of real multiplications per symbol

	Overlap QRM-MLBD	TS-aided QRM-MLBD [12]
QR decomposition	$\{L(4L^2-3L+1)+(2L-1)(N_c-L)(N_c+3L-1)\}/3N_c$	$\{L(4L^2-3L+1)+(2L-1)(N_c-L)(N_c+3L-1)\}/3N_c$
IBI cancellation	$\sqrt{Z}\ (L-1)\ /N_p$	
Computation of $\hat{\mathbf{y}}$,	$2N_c(N_c+2L-1)/X$	$2(N_c+2L-1)$
Path metric calc.	$\sqrt{Z}\ L(2N_c-L+1)/6N_c$ $+\{Z+MZ(N_c-1)\}6N_c/X$	$\sqrt{Z}\ L(2N_c-L+1)/6N_c$ $+\{Z+MZ(N_c-1)\}6$

In this paper, the computational complexity is defined as the number of real multiplications per symbol. The complexities of overlap QRM-MLBD and the conventional QRM-MLBD with CP insertion (TS-aided QRM-MLBD [12]) are shown in Table 1.

In overlap QRM-MLBD, only X ($<N_c$) symbols out of N_c symbols are picked up after QRM-MLBD. Therefore, N_c/X times higher complexity is required for calculating $\hat{\mathbf{y}}$ and the squared Euclidean distance compared to the CP insertion case.

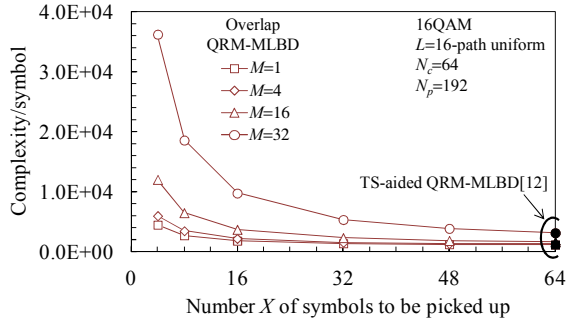

Figure 8. Impact of X on complexity.

Figure 8 shows the complexity as a function of X. In the conventional QRM-MLBD with CP insertion, the number of QRM-MLBD processing is equal to that of overlap QRM-MLBD using X=64. Therefore, the complexity of the QRM-MLBD with CP insertion is almost equal to that of overlap QRM-MLBD using X=64. It can be seen from Fig. 8 that the complexity increases as X decreases. As mentioned in Sect III-A, the required X for achieving higher throughput than the conventional QRM-MLBD with CP insertion is X=16 when $M\geq$4. As a consequence, the computational complexity becomes about 1.3 times higher than that of the conventional QRM-MLBD with CP insertion (TS-aided QRM-MLBD using M=16 when N_c=64 and N_g=16 [12]). The overlap QRM-MLBD achieves about 1.25 times higher peak throughput than the conventional QRM-MLBD with CP insertion. The required X for achieving the peak throughput is X=8 when $M\geq$16. Consequently, the computational complexity increases by about 3.9 times than that of the QRM-MLBD with CP insertion.

IV. Conclusions

In this paper, we proposed an overlap QRM-MLBD which requires no CP insertion. The IBI exists only near the end of the block. Therefore, the IBI can be suppressed by picking up only the reliable symbols after QRM-MLBD. To detect a continuously transmitted symbol stream, the present observation window overlaps with previous and next observation windows. We showed that the overlap QRM-MLBD achieves higher throughput by about 1.25 times than the conventional QRM-MLBD with CP insertion (N_c=64 and N_g=16). The complexity about 3.9 times higher is necessary than the conventional QRM-MLBD (N_c=64) with CP insertion.

References

[1] W. C., Jakes Jr., Ed,. *Microwave mobile communications*, Wiley, New York, 1974.

[2] J. G. Proakis, and M Salehi, *Digital communications*, 5th ed., McGraw-Hill, 2008.

[3] D. Falconer, S. L. Ariyavisitakul, A. Benyamin-Seeyar, and B. Edison, "Frequency domain equalization for single-carrier broadband wireless systems," IEEE Commun. Mag., Vol. 40, No. 4, pp. 58-66. Apr. 2002.

[4] F. Adachi, T. Sao, and T. Itagaki, "Performance of multicode DS-CDMA using frequency domain equalization in a frequency selective fading channel," IEE Electronics Letters, Vol. 39, No.2, pp.239-241, Jan. 2003.

[5] F. Adachi and K. Takeda, "Bit error rate analysis of DS-CDMA with joint frequency-domain equalization and antenna diversity combining," IEICE Transactions on Communications, vol. E87-B, no. 10, pp. 2991–3002, 2004.

[6] K. Nagatomi, K. Higuchi, and H. Kawai, "Complexity reduced MLD based on QR decomposition in OFDM-MIMO multiplexing with frequency domain spreading and code multiplexing." Proc. IEEE Wireless Communications and Networking Conference (WCNC), Apr. 2009.

[7] T. Yamamoto, K. Takeda, and F. Adachi, "Single-carrier transmission using QRM-MLD with antenna diversity," Proc. The 12th International Symposium on Wireless Personal Multimedia Communications (WPMC 2009), Sept. 2009.

[8] H. Moroga, T. Yamamoto, and F. Adachi, "Comparison between time and frequency-domain QRM-ML block signal detection for single-carrier transmission," (in Japanese) IEICE Technical Report, RCS2010-249, pp7-12, Mar. 2011.

[9] I. Martoyo, T. Weiss, F. Capar, and F. K. Jondral, "Low complexity CDMA downlink receiver based on frequency domain equalization," IEEE 58th VTC, Orlando, Florida, USA, Sept. 2003.

[10] T. Takeda, H. Tomeba, and F. Adachi, "Iterative overlap FDE for DS-CDMA without GI," IEEE 64th VTC, Montreal, Quebec, Canada, Sept. 2006.

[11] J. B. Anderson and S. Mohan, "Sequential coding algorithms: A survey and cost analysis," IEEE Trans. on Commun., Vol. 32, pp. 169-176, Feb. 1984.

[12] T. Yamamoto, K. Takeda and F. Adachi, "Frequency-domain block signal detection with QRM-MLD for training sequence-aided single-carrier transmission," EURASIP Journal on Advances in Signal Processing, Vol. 2011.